

Ultrasensitive Detection of Nitrite Based on gold-nanoparticles/ Polyrhodamine B/Carbon Nanotubes Modified Glassy Carbon Electrode with Enhanced Electrochemical Performance

He Xu^{*}, Jiachao Peng, Mengting Zhu, Jianshe Liu

College of Environmental Science and Engineering, Donghua University, Shanghai 201620, P R China

*E-mail: hexu@dhu.edu.cn

Received: 27 July 2017 / Accepted: 5 September 2017 / Published: 12 October 2017

An electrochemical sensing platform based on gold nanoparticles/polyrhodamine B/multi-walled carbon nanotubes composites modified glassy carbon electrode (AuNPs/PRhB/MWCNTs/GCE) was developed for the ultrasensitive determination of nitrite. The morphology and properties of resulting composites were characterized by scanning electron microscopy (SEM) and energy dispersive X-ray spectroscopy (EDX) and electrochemical techniques. Compared with individual PRhB/GCE or MWCNTs/GCE, the AuNPs/PRhB/MWCNTs/GCE sensor exhibited faster electron transfer and better electrocatalytic activity towards the oxidation of nitrite, mainly due to the strong synergistic effect of conducting polymer, metal nanoparticles and carbon nanotubes. Oxidation of nitrite was effectively electrocatalyzed at AuNPs/PRhB/MWCNTs/GCE with significant increase in oxidation current (109%, 79% and 53% in comparison with PRhB/GCE, MWCNTs/GCE and PRhB/MWCTs/GCE) and with considerable decrease in the oxidation potential (0.124, 0.118 and 0.111 V in comparison with PRhB/GCE, MWCNTs/GCE and PRhB/MWCTs/GCE, respectively). The oxidation peak current of nitrite was linearly proportional to its concentration with multi-linear ranges of 1 ~ 25 μM ($R^2 = 0.9922$) and 35 μM ~10 mM ($R^2 = 0.9947$) by differential pulse voltammetry (DPV). Lower concentration of nitrite was detected by amperometry with the linear ranges of 0.1 ~ 5 μM ($R^2 = 0.9973$) and 0.02 ~ 0.16 μM ($R^2 = 0.9994$), and the limit of detection was as low as 6.7 nM ($S/N = 3$). Furthermore, the constructed sensor demonstrated the long-term stability, good reproducibility and excellent anti-interference properties, and it was successfully applied in analysis of nitrite in real samples and gained good testing recoveries of 99% ~ 104.5%.

Keywords: electrochemical oxidation; nitrite; polyrhodamine B; electrodeposition; chemical modified electrode

1. INTRODUCTION

Nitrite ion (NO_2^-) has been widely used for food additive and corrosion inhibitor, and it has been recognized as an alarming pollutant to the human health and environment. It can easily interact

with blood hemoglobin and lead to the irreversible oxidation of hemoglobin to methemoglobin. In addition, it is well known that nitrite can react with amines and amides to form highly carcinogenic N-nitrosamine compounds [1]. The World Health Organization has reported that the fatal dose of nitrite ingestion is between 8.7 μM and 28.3 μM . Therefore, it is necessary to accurately and rapidly detect nitrite with high sensitivity and selectivity for environmental security and public health.

Many methods have been developed for quantitative detection of nitrite such as spectrophotometry [2], chemiluminescence [3], high-performance liquid chromatography [4], capillary electrophoresis [5] and etc.. None is universally satisfactory. These traditional methods are reliable but time-consuming, complicated, expensive, and are also difficult to perform on-site [6]. As an alternative method for nitrite detection, the electrochemical methods have been proven to be a rapid and powerful technique for the determination of trace nitrite due to its fast procedure, low cost, good selectivity, high accuracy and real-time analysis, particularly providing a relatively safe and environmentally friendly approach with fewer reagents involved [7]. Unfortunately, the electrochemical oxidation of nitrite at the traditional electrodes requires a high overvoltage where oxidable compounds (such as nitrite oxidation products and intermediate) may inhibit electrode processes via irreversible adsorption on the electrode surface, and the electrodes tend to be poisoned by the products generated during the electrochemical process [8].

To resolve these problems, one strategy is to use various functionally electron-transfer materials in the construction of the working electrode to modify electrode surface to decrease overpotential and improve the sensitivity [9]. Remarkably, conducting polymers that possess high electrical conductivity can act as redox mediators with direct charge transport features, which are of increasing scientific and technological interest for the development of electrochemical sensors. Up to date, various conducting polymers, such as azines, have been reported for nitrite electrooxidation by in situ electropolymerization of their monomers at a bare electrode, including azur A [10], methylene blue [11], methylene green [12], neutral red [13], toluidine blue [14] and so on. These conducting polymers have good characteristics of high mechanical flexibility, low cost, ease of synthesis and sites specific growth capability. Rhodamine derivatives as a group of xanthene dyes possess excellent spectroscopic properties, which have been commonly used for fluorescent labeling reagents, dyes laser source, and degradants in bioanalytical chemistry and photoelectrocatalysis [15, 16]. Few PRhB based polymer films are reported as redox mediators for developing electrochemical sensors. In 2014 year, Lu and Qiu reported an electropolymerized Rhodamine B sensing film for nitrite detection by electrochemical oxidation [17]. However, only polyrhodamine B modified glassy carbon electrode (PRhB/CNTs) was confronted with the challenges of low sensitivity and stability, high over oxidation potential and poor anti-fouling properties. The electro-oxidation potential was still high (0.96 V) for nitrite detection [17], and the electrodes tend to be poisoned by the generated products. Importantly, the polyrhodamine B film could not adhere well on the GCE substrate, and it easily broke off from GCE when it was reused multiply, impacting on sensitivity, stability and reproducibility for electrochemical detection of nitrite in real applications.

To overcome these problems, another strategy is to use excellent supporting materials as matrix for the electropolymerization of RhB on the electrode surface. Carbon nanotubes (CNTs) are known as sp^2 hybridized hollow cylindrical carbon nanomaterial, have been used as a promising material in

different applications. Particularly, multi-walled carbon nanotubes (MWCNTs) have high specific surface area, good conductivity and strong adsorption ability, wide potential window and chemical inertness, which enable it to be used as an excellent matrix for the immobilization of nano-composites and the improvement of electrocatalytic activity [18, 19]. On another front, noble metal nanostructures were usually doped into the conducting polymer or carbon substrate materials to enhance sensitivity for the detection nitrite. Au nanoparticles have been extensively exploited for the determination of nitrite due to its remarkable conductivity, well electrocatalytic ability, unique dimensions, high effective surface area and biocompatibility [20, 21]. It is worth noting that Au nanoparticles could be modified with some supporting materials to achieve great selectivity, sensitivity, and stability for analytes detection [22].

In this paper, MWCNTs were introduced as supporting substrate to electropolymerize Rhodamine B, and gold nanoparticles were doped into PRhB/MWCNTs composites by electrodeposition, which developed a new matrix as the sensor platform for ultrasensitive detection of nitrite. The proposed AuNPs/PRhB/MWCNTs/GCE sensor exhibited faster electron transfer rate, more electroactive areas and higher conductivity, which were attributed to accelerating the electrooxidation of nitrite. Oxidation potential of nitrite at AuNPs/PRhB/MWCNTs/GCE was obviously decreased and oxidation peak current was significantly improved in comparison with those at PRhB/GCE or MWCNTs/GCE, owing to synergic effect of MWCNTs, gold nanoparticles and conducting polymer. The analytical performance of AuNPs/PRhB/MWCNTs/GCE was evaluated and obtained with low over-potential of nitrite, wide linear range, low detection limit, excellent anti-fouling properties, good reproducibility and stability, suggesting that the constructed sensor would offer a promising candidate to detect nitrite in application with high efficiency.

2. EXPERIMENTAL

2.1 Regents and Materials

HAuCl₄·6H₂O, Rhodamine B, NaNO₂, K₄[Fe(CN)₆], K₃[Fe(CN)₆], N, N-dimethyl formamide (DMF) were purchased from Sinopharm Chemical Reagent Co. (Shanghai, China), MWCNTs were obtained from Pioneer Nanotechnology Co. (Nanjing, China), and were functionally carboxyl-pretreated before use. The supporting electrolyte used was phosphate buffer solution (PBS) of various pH, and prepared by 0.1 M KH₂PO₄ and 0.1 M K₂HPO₄ in doubly distilled water. All the chemicals were of analytical reagent grade and used without further purification.

2.2 Apparatus

Electrochemical experiments were performed with CHI760E electrochemical workstation (Shanghai Chenhua Co., China) with a conventional three-electrode cell. A modified glassy carbon electrode was used as working electrode. A saturated calomel electrode (SCE) and a platinum wire were used as reference electrode and auxiliary electrode, respectively. Scan electron micrographs

(SEM) were obtained with a field emission scanning electron microscope (S-4800, Japan). All electrochemical experiments were performed in N₂ atmosphere at room temperature.

2.3 Preparation of AuNPs/PRhB/MWCNTs modified GCE

A bare glassy carbon electrode was polished carefully to a mirror-like surface with 0.05 μmol/L alumina aqueous slurry and then successively washed in an ultrasonic cleaner with nitric acid (1:1), anhydrous ethanol and distilled water. The fresh bare GC electrode was pretreated in 0.5 M H₂SO₄ solution at a scan rate of 100 mV/s, and then the CVs of bare GCE were recorded in 5 mM [Fe(CN)₆]^{3-/4-} containing 0.1M KCl until a pair of well-defined redox peaks were observed. Next, 2.0 mg MWCNTs were dispersed in 1mL DMF with the aid of ultrasonic agitation to give 2.0 mg/mL black suspension. 5 μL MWCNTs of solution was cast on the surface of fresh GCE and then the solvent DMF was evaporated to form a MWCNTs-modified GCE (MWCNTs/GCE).

PRhB/MWCNTs/GCE was prepared by electropolymerization of Rhodamine B at the MWCNTs/GCE substrates according to references [17]. Briefly, the above-mentioned MWCNTs/GCE was submerged in a 0.1 M K₂HPO₄-KH₂PO₄ (pH 5.0) solution containing 0.25 mM Rhodamine B and 0.3 M NaNO₃. The PRhB film was electrochemically deposited onto the MWCNTs/GCE by cyclic voltammetry with the applied potential ranging from -1.4 to 1.8 V at a scan rate of 50 mV/s for several scans. The PRhB/GCE were electropolymerized by the same procedure without MWCNTs.

The Au nanoparticles were also electrodeposited onto the PRhB/MWCNTs/GCE by cyclic voltammetry. The PRhB/MWCNTs/GCE as working electrode was immersed in a 0.1 M K₂HPO₄-KH₂PO₄ (pH 2.2) solution containing 1mM HAuCl₄. Then 20 consecutively cyclic voltammograms were performed in the potential range from 0.1 V to -1.1 V with scan rate of 50 mV/s. The resulting AuNPs/PRhB/MWCNT/GCE was dried in air oven and used for further electrochemical studies.

2.4 Electrochemical measurements

Cyclic voltammetry was used to study the electrochemical reaction of nitrite and carried out in the potential ranging from 0.0 V to 1.2 V at a scan rate of 50 mV/s. Different pulse voltammetry was recorded for the detection of nitrite from 0.2 V to 1.2 V with pulse amplitude of 50 mV, pulse width of 5 s and pulse period of 0.5 s. Low concentration of nitrite was detected by amperometric current-time (i - t) curve, which was performed in a stirring 0.1 M PBS (pH 3.5) solution at an applied potential of 0.80 V .

3. RESULTS AND DISCUSSION

3.1 Morphologic Characterization

Figure 1 shows the SEM images of (A) PRhB/MWCNTs and (B) AuNPs /PRhB/MWCNTs. As seen in Figure 1A, PRhB film deposited on the MWCNTs/GCE was obviously visible as a gray deposit covering a large proportion of the surface of MWCNTs, and the accumulated PRhB film was relatively

uniform in term of thickness and distribution over the surface of MWCNTs. Figure 1B shows the SEM image of AuNPs/PRhB/MWCNTs modified GCE. From the image shown in Figure 1B, Au nanoparticles mainly consisted of spherical nanostructures having relatively uniform size, which were well dispersed on the PRhB/MWCNTs surface without obvious agglomerations. The average size of Au nanoparticle was approximately 30-50 nm. The spherical nanostructures of AuNPs may possess larger surface area and more active sites, which may lead to the enhancement of catalytic performances toward the oxidation of NaNO_2 . EDX (Figure 1C) were further employed to examine the chemical composition of the obtained composites with C and Au.

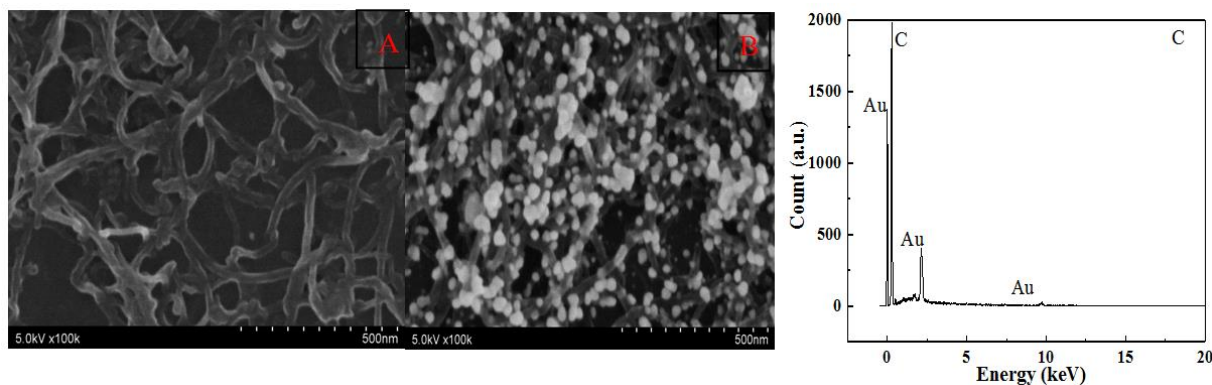


Figure 1. SEM images of (A) PRhB/MWCNTs and (B) AuNPs/PRhB/MWCNTs; (C) Energy-dispersive X-ray (EDX) spectroscopy of AuNPs/PRhB/MWCNTs.

3.2 Electrochemical polymerization of Rhodamine B at GCE and MWCNTs/GCE

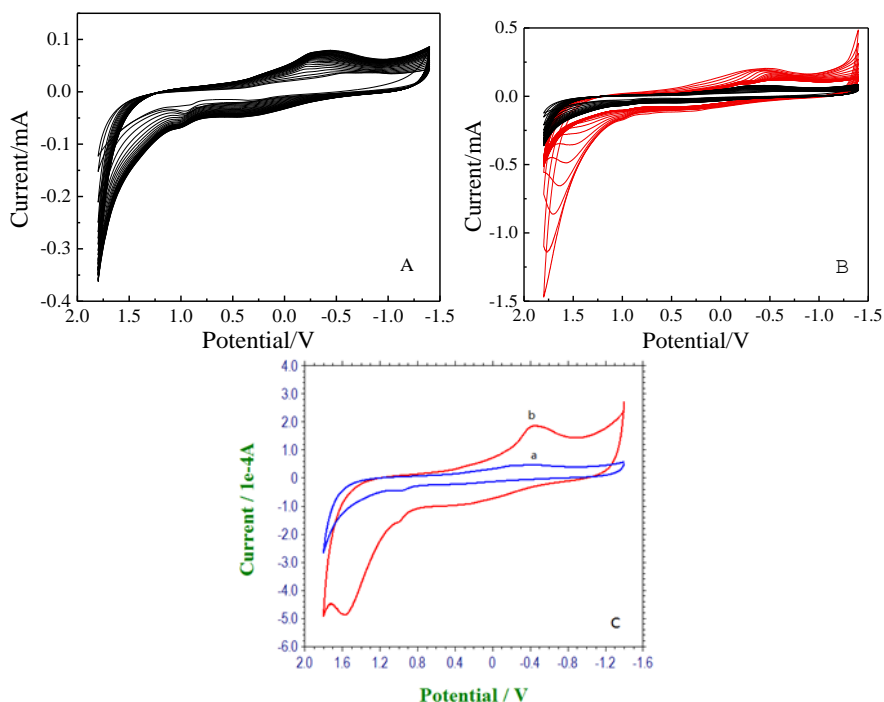


Figure 2. Cyclic voltammograms of 0.25 mM Rhodamine B at (A) bare GCE and (B) MWCNTs/GCE (red line, black lines are at bare GCE) in 0.1 M PBS (pH 5.0) containing 0.3 M NaNO_3 . (C) Unicyclic voltammograms of electropolymerization for 0.25 mM Rhodamine B from 9 to 10 circles at (a) bare GCE and (b) MWCNTs/GCE. Scan rate: 50 mV/s

To determine the better electrochemical properties of PRhB at the MWCNTs surface as supporting matrix, the electropolymerization of rhodamine B at different substrates was investigated. Figure 2 displays that the electrochemical polymerization processes were carried out at (A) bare GCE (black line) and (B) MWCNTs/GCE (red line, black lines are at bare GCE) by cyclic potential sweep from -1.4 to 1.8 V with a scan rate of 50 mV/s in PBS (pH 5.0) containing 0.25 mM Rhodamine B and 0.3 M NaNO₃. As seen in Figure 2, both of the redox peak currents were continually increased with the successive scans in the potential from -1.4 to 1.8 V at bare GCE (A) and MWCNTs/GCE (B), indicating that Rhodamine B is well electropolymerizing on the GCE (A) and MWCNTs/GCE (B) surface, respectively. However, the peak currents of electropolymerization process were much higher at the MWCNTs/GCE (red line) than those at bare GCE (black line). Figure 2C shows that the unicyclic scan curve of electropolymerization process for Rhodamine B from 9 to 10 is recorded at (a) bare GCE and MWCNTs/GCE. Compared with the only PRhB modified GCE as reported previously [17], the peak currents of the electropolymerization of Rhodamine B at the MWCNTs/GCE were improved about 2-folds for oxidation and 3-folds for reduction, respectively. The results demonstrated that MWCNTs provided more electroactive sites, higher specific surface area, and better conductivity than those of bare GCE, and resulted in an improvement that Rhodamine B would be electropolymerized more easily [23]. In addition, the strong absorptive ability and large electroactive performance of MWCNTs attracted Rhodamine B from bulk solution to electrode surface [24]. Therefore, MWCNTs were result into the better substrate and matrix for Rhodamine B electrodeposition, which would improve the sensitivity, stability and electrocatalytic properties for nitrite detection in further study.

3.3 Electrochemical characterization of AuNPs/PRhB/MWCNTs/GCE

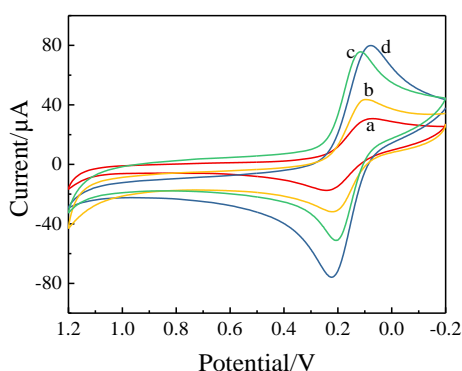


Figure 3. Cyclic voltammograms of (a) PRhB/GCE, (b) bare GCE, (c) PRhB/MWCNTs/GCE and (d) AuNPs/PRhB/MWCNTs/GCE in 5 mM [Fe(CN)₆]^{3-/4-} containing 0.1 M KCl solution with a scan rate of 50 mV/s.

It is well known that cyclic voltammetry is a powerful tool to verify increased electron transfer rate and high electroactive area for different modified electrodes. Figure 3 represents steady-state cyclic voltammograms for the (a) PRhB/GCE, (b) bare GCE, (c) PRhB/MWCNTs/GCE and (d) AuNPs/PRhB/MWCNTs/GCE in 5 mM [Fe(CN)₆]^{3-/4-} and 0.1 M KCl solution at 50 mV/s. In the case

of bare GCE (curve b), the redox peaks of $[\text{Fe}(\text{CN})_6]^{3-/4-}$ were well-defined, which illustrated that the GCE surface was satisfactory through pretreatment in H_2SO_4 solution. On the contrary, after electropolymerization of Rhodamine B, the peak currents of $[\text{Fe}(\text{CN})_6]^{3-/4-}$ at the PRhB/GCE were oppositely declined (curve a). When MWCNTs were introduced as supporting matrix for PRhB electropolymerization, the redox current response of $[\text{Fe}(\text{CN})_6]^{3-/4-}$ at the PRhB/MWCNTs/GCE was increased again. Furthermore, the AuNPs/PRhB/MWCNTs/GCE exhibited largest peak current response of $[\text{Fe}(\text{CN})_6]^{3-/4-}$ in the same condition. Interestingly, the oxidation current response of $[\text{Fe}(\text{CN})_6]^{3-/4-}$ at the AuNPs/PRhB/MWCNTs/GCE was about 4.5 times, 3.5 times and 1.5 times greater than those at PRhB/GCE, bare GCE and PRhB/MWCNTs/GCE, respectively. This fact may be explained that only PRhB film at bare GCE was too thick and compact for consecutive 30 scans by cyclic voltammetry according to reference [17], which might hinder the electron transfer of ferricyanide toward the bare GCE surface. When MWCNTs were introduced into the bare GCE surface (curve c), MWCNTs would provide a large accessible surface area, and the fast-oriented transmission of charges as excellent matrix for sensing. The electropolymerization of Rodamine B could be carried out more easily, and more homogeneous and well-dispersed PRhB films were obtained [23, 24], and the current response of $[\text{Fe}(\text{CN})_6]^{3-/4-}$ at PRhB/MWCNTs/GCE was improved again. In addition, unique property of gold nanoparticles was also attributed to accelerating the electron transfer rate of $[\text{Fe}(\text{CN})_6]^{3-/4-}$ toward electrode surface [20], and the proposed AuNPs/PRhB/MWCNTs/GCE provided best current response of $[\text{Fe}(\text{CN})_6]^{3-/4-}$. According to Randles-Sevcik equation [25]:

$$I_p = 2.69 \times 10^5 AD^{1/2} n^{3/2} \gamma^{1/2} C$$

where n is the number of electrons participating in the redox reaction, A is the area of the electroactive area (cm^2), D is diffusion coefficient of the molecule in solution (cm^2/s), and γ is the scan rate of the potential perturbation (V/s). The $[\text{Fe}(\text{CN})_6]^{3-/4-}$ redox system used in this study is one of the most extensively studied redox couples in electrochemistry and exhibits a heterogeneous one-electron transfer ($n = 1$). C is equal to 5 mM, and the diffusion coefficient (D) is $(6.7 \pm 0.02) \times 10^{-6} \text{ cm}^2/\text{s}$. The average values of the electroactive surface areas for optimized PRhB/GCE, bare GCE, PRhB/MWCNTs/GCE and AuNPs/PRhB/MWCNTs/GCE were 0.053 cm^2 , 0.071 cm^2 , 0.183 cm^2 and 0.251 cm^2 , respectively. It verified that the fastest electron transfer rate and highest electroactive area were obtained at the AuNPs/PRhB/MWCNTs/GCE, and a sure sign of the enhanced electrocatalytic performance of the proposed method was demonstrated.

3.4 Electrocatalytic behavior of nitrite at AuNPs/PRhB/MWCNTs/GCE

The electrocatalytic behavior of the AuNPs/PRhB/MWCNTs/GCE towards nitrite oxidation was studied by cyclic voltammetry. Figure 4A shows that the typical CVs of (a) PRhB/GCE, (b) MWCNTs/GCE, (c) PRhB/MWCNTs/GCE and (d) AuNPs/PRhB/MWCNTs/GCE in 0.1 M PBS (pH 3.5) with 3 mM NaNO_2 . As can be seen, the oxidation of nitrite occurred at 0.80 V at PRhB/GCE and the oxidation peak potential was at more than 0.90 V ((curve a), 0.96 V in reference reported previously [17]). When the oxidation of nitrite occurred at MWCNTs/GCE and

PRhB/MWCNTs/GCE, the oxidation peak potentials negatively shifted to 0.809 V and 0.802 V, respectively.

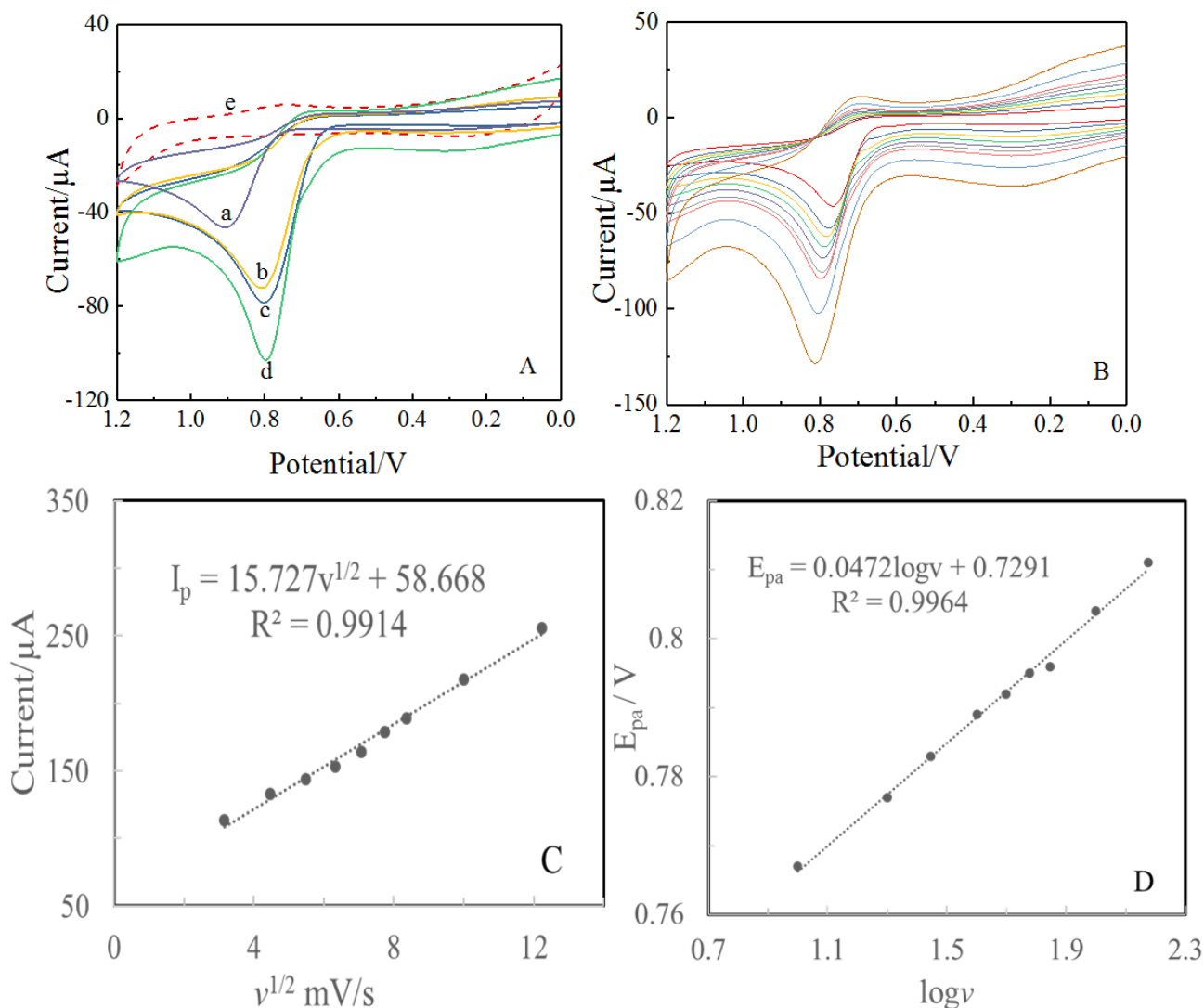


Figure 4. (A) Cyclic voltammograms of (a) PRhB/GCE, (b) MWCNTs/GCE, (c) PRhB/MWCNTs/GCE and (d, e) AuNPs/PRhB/MWCNTs/GCE in the presence of 0 mM (e) and 3 mM (a \rightarrow d) NaNO_2 in 0.1 M PBS (pH 3.5) with potential ranging from 0.0 V to 1.2 V at a scan rate of 50 mV/s. (B) Cyclic voltammograms of AuNPs/PRhB/MWCNTs/GCE in 0.1 M PBS (pH 3.5) containing 3 mM NaNO_2 at different scan rates (from inner to outer: 10, 20, 30, 40, 50, 60, 70, 100, 150 mV/s). The plots of oxidation peak current versus $v^{1/2}$ (C) and peak potential versus $\log v$ (D).

At AuNPs/PRhB/MWCNTs/GCE, the electrochemical oxidation of nitrite occurred at 0.60 V, and the peak current appeared at 0.796 V, suggesting that the oxidation over-potential of nitrite was dramatically decreased compared with that obtained at individual PRhB/GCE. The oxidation peak currents were remarkably improved about 53%, 79% and 109% at the (b) MWCNTs/GCE, (c) PRhB/MWCNTs/GCE and (d) AuNPs/PRhB/MWCNTs/GCE, respectively. No current response was obtained at the AuNPs/PRhB/MWCNTs/GCE without nitrite (curve e). The highest current response

and the smallest peak potential were obtained at AuNPs/PRhB/MWCNTs/GCE, indicating that the proposed sensor had the best electrocatalytic performance for the oxidation of nitrite.

In order to investigate the reaction kinetics, the effects of scan rate on the oxidation peak potential and current were evaluated by cyclic voltammetry at different scan rates. Figure 4B represents the CVs of AuNPs/PRhB/MWCNTs/ GCE in 0.1 M PBS (pH = 3.5) solution with 3 mM NaNO₂ at the different scan rates of 10-150 mV/s. The cyclic voltammograms show clear well-defined irreversible oxidation peaks corresponding to the NO₂⁻ electron transfer process [17]. The oxidation peak currents increased linearly with the square root of the scan rate, and the calibration equation was $I_{pa} = 15.727 v^{1/2} + 58.668$ ($R^2=0.9914$), which indicated that the involved electrochemical reaction was controlled by the diffusion step (Figure 4C). It was noted that the oxidation potentials at the AuNPs/PRhB/MWCNTs/GCE slightly shifted to the positive potential when the scan rates were increased and the linear regression equation of E_{pa} versus the logarithm of the scan rate shown in Figure 4D was expressed as $E_{pa} = 0.0472 \log v + 0.7291$ ($R^2=0.9964$). The electron transfer number (n) is calculated according to the following Laviron's equation [25]:

$$E_{pa} = E^{0'} + \left(\frac{RT}{anF}\right) \ln\left(\frac{RTk^0}{anF}\right) + 2.30\left(\frac{RT}{anF}\right) \log v \quad (1)$$

where a is the electron transfer coefficient, n is the number of electron transferred, $E^{0'}$ is the formal potential, v is the scan rate. R , T and F have their conventional meanings. The n values is calculated to be 2.2, when a is taken 0.5 in totally irreversible reaction. It means that about two electrons were involved in the irreversible reaction of NaNO₂. According to the reported references [26, 27] and our analysis, possible electrooxidation mechanism of nitrite in 0.1 M PBS (pH 3.5) on the AuNPs/PRhB/MWCNTs/GCE could be proposed as follows:



3.5 Effect of pH

Apparently, the pH value has an important influence on the sensing of the AuNPs/PRhB/MWCNTs films. In order to obtain a better electrocatalytic activity and reaction kinetics, the effects of pH on the oxidation current and potential of nitrite at AuNPs/PRhB/MWCNTs/GCE were optimized by testing the CVs in 3 mM NaNO₂ solution with various pH (0.1 M PBS) (Figure 5). The peak current obviously increased with the increase of pH from 2.0 to 3.5, and slowly improved from 4.0 to 6.5, but then decreased upon the further increase of pH to 7.0 (Figure 5B). Small peak current at lower pH (pH < 3.0) was attributed to the instability of nitrite anions in strong acidic medium [26] due to the conversion of NO₂⁻ to NO and NO₃, as shown in Eq.(6):



On the other hand, since the pKa of HNO₂ was 3.3, most nitrite anions were protonated in acidic solution. When pH was above 6.5, the electrocatalytic oxidation of nitrite became more difficult due to shortage of proton, and the catalytic peak currents were decreased [27]. Meanwhile, the effect on the oxidation peak potential at the AuNPs/ PRhB/MWCNTs/GCE was also studied (Figure 5C). As expected, the anodic peak potentials decreased at pH 2.0-5.0, and was not seriously affected with the increase of pH in further, which revealed that the proton was involved in the electrocatalytic oxidation of nitrite. As shown in Figure 5A, some oxidable by-products were formed for reversal scan (at the potential range of 0.4 ~ 0.6 V) at the electrode surface under higher pH conditions, which would also inhibit the oxidation process, resulting in the wider peak shape and stronger background current. However, when pH values were lower than 3.5 (2.0, 2.5, 3.0 and 3.5), the E_{pa} and pH values showed a linear relationship, and the fitting regression equation was E_{pa}/V = 0.806 - 0.016 pH (R² = 0.9817). Considering the dissociation constant of HNO₂, oxidation peak current and potential of NO₂⁻, pH 3.5 was chosen for the following analytical experiments.

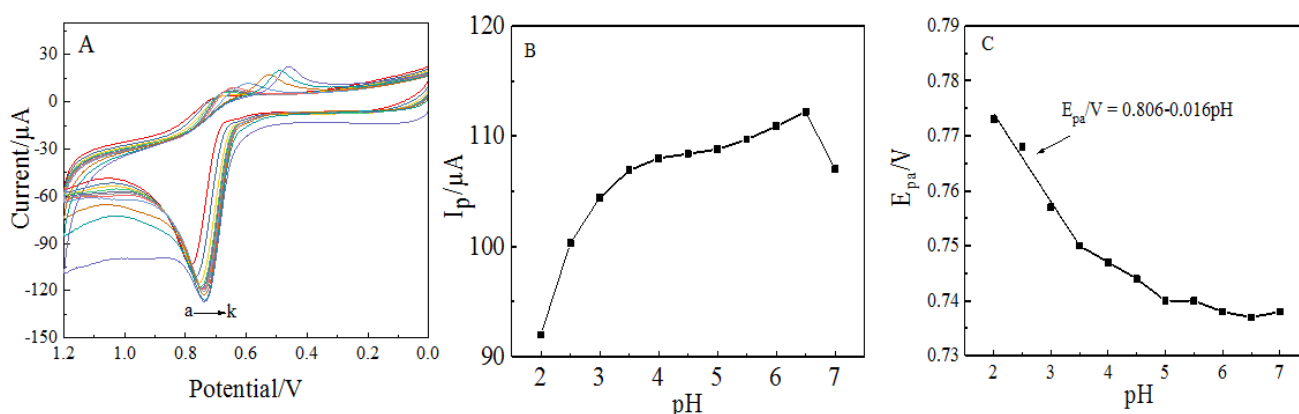


Figure 5. (A) Cyclic voltammograms of AuNPs/PRhB/MWCNTs/GCE in 0.1 M PBS (pH 3.5) containing 3 mM NaNO₂ with the pH ranging from 2.5 to 7.0 (a → k) at a scan rate of 50 mV/s. The plots of anodic peak current (B) and peak potential (C) against pH.

3.6 Differential pulse voltammetric detection of nitrite

Figure 6 describes that the typical DPV curves of AuNPs/PRhB/MWCNTs/GCE in the presence of different NO₂⁻ concentrations in 0.1 M PBS (pH 3.5). As verified in Figure 6, the sizable catalytical currents were observed. The response currents at the AuNPs/PRhB/MWCNTs/GCE were proportional to the concentration of nitrite in the range of 1 ~ 25 μM ($I_{p1} = 87.584C_{\text{NO}_2^-} + 0.1538$, R² = 0.9922) and 35 μM ~ 10 mM ($I_{p2} = 10.236 C_{\text{NO}_2^-} + 5.9854$, R² = 0.9947), and the corresponding sensitivities of the sensors were 87.58 μA·L·mmol⁻¹ and 10.24 μA·L·mmol⁻¹, respectively. The as-prepared AuNPs/PRhB/MWCNTs/GCE provided such wide linear range (1 μM ~ 10 mM) and good sensitivity, which were much more superior to those of only CNTs/GCE [28], AuNPs modified electrode [29] and PRhB/GCE [17]. Meanwhile, it shows a comparable performance to others previously reported methods by DPV, such as gold nanoparticles/1-pyrenemethylamine/graphene oxide/carbon nanotubes composites modified electrode [30], silver/carbon nano-composites electrode

[31], PdCo alloy nanoparticles-embedded carbon nanofiber electrode [32], gold nanoparticles/flower-like graphene coated electrode [26], poly(vinylferrocenium)/multi-walled carbon nanotubes coated electrode [33], Cu nanoparticles/multiwall carbon nanotubes/reduced graphene oxide electrode [34], Fe₂O₃ nanoparticles/reduced graphene oxide nanosheets modified electrode [35], and so on. However, these reported methods need complicated materials and time-consuming preparation. It was noteworthy that the sensitivity for the detection of low concentration of nitrite was higher than that of high concentration. We believe that it is due to the cooperative effect of carbon nanotubes, metal nanoparticles and conducting polymer, and the proposed method has its specific advantage and better properties for the detection of low concentration of nitrite.

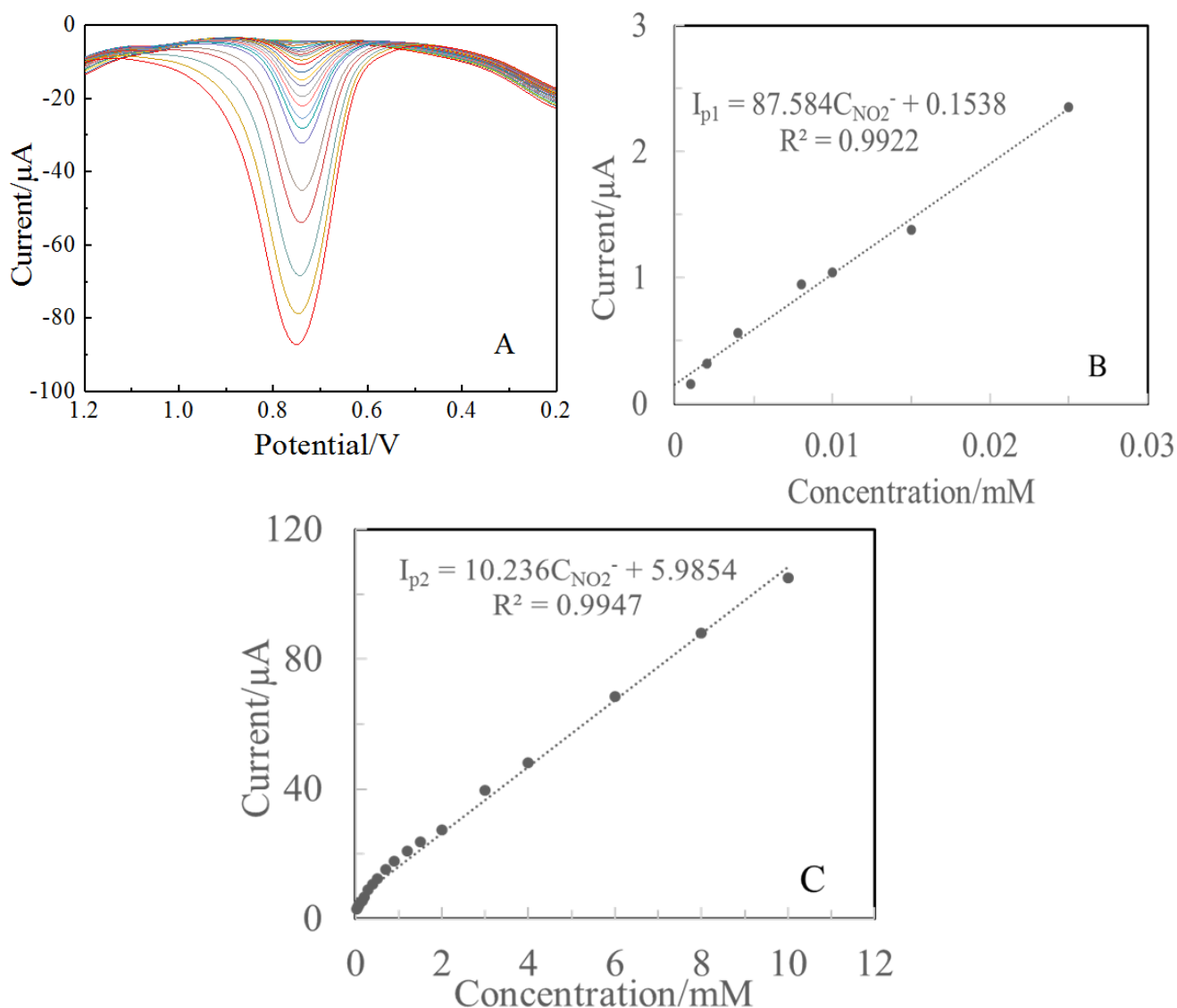


Figure 6. (A) DPV curves of the AuNPs/ PRhB/MWCNTs/ GCE in 0.1 M PBS (pH 3.5) solution containing different concentrations of NaNO₂. The relationship between oxidation peak currents versus the concentration of NaNO₂ from 1 ~ 25 μM (B) and 35 μM ~ 10 mM (C).

3.7 Amperometric determination of nitrite

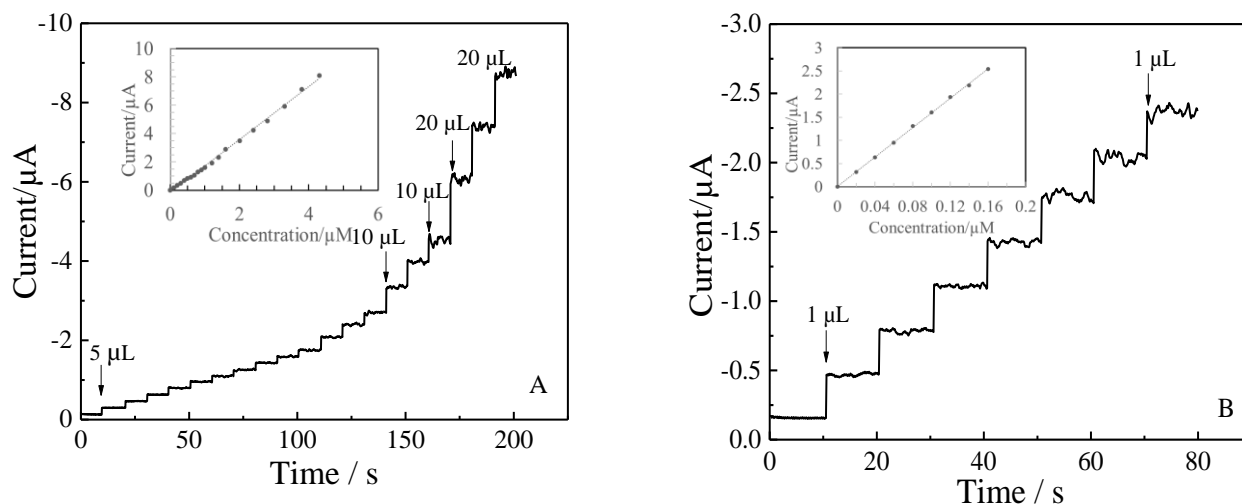


Figure 7. (A) Amperometric response on the AuNPs/PRhB/MWCNTs/GCE with successive injection of different volumes of 0.2 mM NaNO₂ (A) (5 μL, 10 μL, 20 μL) and (B) (1 μL) in 10 mL of 0.1 M PBS (pH 3.5) at the potential of 0.80 V under stirring PBS solution (inset graphs are plot of oxidation peak current versus NO₂⁻ concentration from 0.1 ~ 5 μM (A) and 0.02 ~ 0.16 μM (B)).

It is generally known that amperometry is preferred technique for trace analytes detection because it provides a fast evaluation of the sensor and contributes the main sensor characteristics such as sensitivity and response time. In order to investigate the performance of the proposed AuNPs/PRhB/MWCNTs/ GCE, low concentration of nitrite for detection was studied by amperometry. Figure 7 displays the typical amperometric response of AuNPs/PRhB/MWCNTs/ GCE upon successive addition of different concentrations of nitrite in 0.1 M PBS (pH 3.5) at an applied potential of 0.8 V. When an aliquot of NO₂⁻ was added into the stirring PBS solution, AuNPs/PRhB/MWCNTs/GCE responded rapidly to the substrate and the current rose steeply to reach a stable value. The modified electrode accomplished 95 % of the steady-state current within 2 s, revealing a fast amperometric response behavior. The response currents at the AuNPs/PRhB/MWCNTs/GCE were proportional to the concentration of nitrite in the range of 0.1 ~ 5 μM ($R^2 = 0.9973$) (Figure 7A). Meanwhile, it can be clearly seen that the oxidation peak current of nitrite with their lower concentrations of 0.02 ~ 0.16 μM showed a better linear relationship with a correlation coefficient of 0.9994 (Figure 7B). Based on the confidence limits of the regression equation and for a signal -to-noise of 3, the limit of detection was as low as 6.7 nM. The analytical performance of the proposed electrode and other electrodes for the detection of nitrite are compared and listed in Table 1. It can be observed that the AuNPs/PRhB/MWCNTs/ GCE in this study presents the comparable performance with most of the reported nitrite sensors, where it is necessary to use electron mediators or even more complex materials. The linear range and detection limit of the proposed electrode are more favorable or comparable than those of individual PRhB/GCE [17], myoglobin/Au nanoparticle/carbon nanotube/polytyramine composites modified GCE [36], chitosan/Pt

nanoparticles/carbon nanotubes/phosphomolybdate nanocomposite electrode [37], urchin-like palladium/carbon nanotubes thin film electrode [38], Pt nanoparticles/polyaniline/graphene nanocomposites electrode [39], silver nanoparticles/P(MMA-co-AMPs) modified electrode [40], poly(Toluidine blue O)/carbon nanotubes electrode [41], polyoxometalate[PMO₁₁O₃₉]₇/carbon nanocomposites electrode [42], AuPd/UiO-66-NH₂ metal-organic framework modified electrode [43], Au-Pt bimetallic nanoparticles/nitrogen-doped graphene modified electrode [44], Au-Pd nanostructures/reduced graphene oxide electrode [45], horseradish peroxidase/porous Co₃O₄ nanosheets/reduced graphene oxide modified electrode [46] and so on. The enhanced electrochemical performance of the proposed AuNPs/PRhB/MWCNTs/ GCE may be related to the high surface-to-volume ratio with more active sites and larger electrochemical area by using MWCNTs as supporting materials. In addition, such good sensitivity and fast response can be attributed to the efficiency of the electron transfer between AuNPs/PRhB/MWCNTs modified electrode and nitrite due to the catalytical effect resulting from synergism coupling effect of gold nanoparticles, MWCNTs and conductive polymer. Importantly, the proposed method is a simple, convenient and rapid technique for electrocatalytical detection of nitrite, implying that AuNPs/PRhB/MWCNTs composites as promising materials were deserved to be promoted in nitrite detection.

3.8 Selectivity, stability and reproducibility

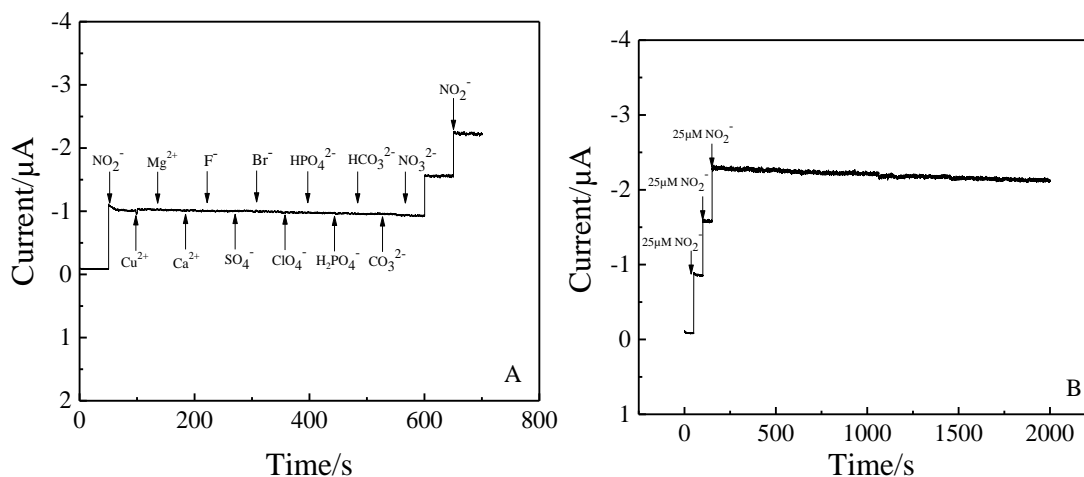


Figure 8. (A) Amperometric response at the AuNPs/PRhB/MWCNTs/GCE to successive additions of the interferences into stirred PBS (pH 3.5) in presence of 25 μM nitrite at 0.8 V. (B) Amperometric response at the AuNPs/PRhB/MWCNTs/GCE for the addition of 25 μM nitrite into continuously stirred PBS and the amperometric response up to 2000 s.

The selectivity of the sensor is more important to further access for real-time sensing in water samples, since other metal cations and anions could interfere or be active on the fabricated electrode surface. Hence, the selectivity of the AuNPs/PRhB/MWCNTs/GCE was evaluated for the detection of nitrite in the presence of 50-fold metal cations and anions by amperometry. Figure 8A shows the effect of different ions as the interferences on the electrooxidation of nitrite at the

AuNPs/MWCNTs/PRhB/GCE. It can be seen clearly that 50-fold concentration of Cu^{2+} , Mg^{2+} , Ca^{2+} , F^- , SO_4^{2-} , Br^- , ClO_4^- , HPO_4^{2-} , $\text{H}_2\text{PO}_4^{2-}$, HCO_3^- , CO_3^{2-} and NO_3^- ions did not show any response on the modified electrode. The proposed electrode has high selectivity towards the detection of nitrite in the presence of common metals ions and anions. The operational stability of AuNPs/PRhB/MWCNTs/GCE was further examined by amperometry and the results were shown in Figure 8B. It obviously revealed that only 3.3% of its initial current response was lost when it continuously ran up to 2000 s in 25 μM nitrite solution. The storage stability of AuNPs/PRhB/MWCNTs/GCE was also studied towards the detection of 25 μM nitrite by DPV. Its current response had almost no change for first 7 days and retained 98% of the initial response current towards nitrite detection after 30 days storage in air. The repeatability and reproducibility of the proposed sensor were examined for the detection of 25 μM nitrite. The relative standard deviation (RSD) for 15 successive determinations of nitrite was found 1.4% and 5 independent electrodes was found 2.3%. The reproducibility and stability of the AuNPs/PRhB/MWCNTs/GCE were superior to those of PRhB/GCE [17], which were more favorable for the detection of nitrite in real applications.

3.9 Determination of nitrite ions in real samples

To demonstrate the feasibility of the present sensor applied to the practical samples, the detection of nitrite in tap water and lake water was performed. The water samples were filtered and used for the real sample analysis. A standard addition method was adopted to find the recoveries and the results were shown in Table 2. It can be clearly observed that the developed sensor produced satisfactory recoveries from 99% to 104.5 %, which implied that the proposed method was reliable for the detection of nitrite in environmental samples.

Table 1. Comparison of several typical electrochemical properties for NaNO_2 detection

Modified Materials	Technique	Linear Range	Limit Detection	Ref.
Carbon nanotubes	DPV	2 ~ 10 μM 20 μM ~ 1 mM	0.5 μM	[28]
AuNPs	CV	10 ~ 5000 μM	2.4 μM	[29]
gold nanoparticles/1-pyrenemethylamine/graphene oxide/carbon nanotubes	DPV	2 μM ~ 10 mM	0.67 μM	[30]
silver/carbon nanocomposites	DPV	4 μM ~ 2 mM	0.48 μM	[31]
PdCo alloy nanoparticles-embedded carbon nanofiber electrode	DPV	0.4 ~ 400 μM	0.2 μM	[32]
gold nanoparticles/flower-like graphene	DPV	0.125 μM ~ 20.375 mM	0.01 μM	[26]
poly(vinylferrocenium)/multi-walled carbon nanotubes	DPV	1 ~ 400 μM	0.1 μM	[33]
Cu nanoparticles/multiwall	DPV	0.1 ~ 75 μM	30 nM	[34]

carbon nanotubes/reduced graphene oxide				
Fe ₂ O ₃ nanoparticles/reduced graphene oxide nanosheets	DPV	0.05 μM ~ 0.78 mM	15 nM	[35]
myoglobin/Au nanoparticle/carbon nanotubes/polytyramine	Amperometry	1 ~ 8000 μM	0.002 μM	[36]
chitosan/Pt nanoparticles/carbon nanotubes/phosphomolybdate nanocomposite	Amperometry	0.125 μM ~ 4.167 mM	3.8 nM	[37]
urchin-like palladium/carbon nanotubes thin film electrode	Amperometry	2 ~ 238 μM / 283 ~ 1230 μM	0.25 μM	[38]
Pt nanoparticles/polyaniline/graphene nanocomposites	Amperometry	0.4 μM~0.99 mM/0.99 mM ~ 7.01 mM	0.13 μM	[39]
silver nanoparticles/P(MMA-co-AMPs)	Amperometry	1 μM ~ 10 mM	0.2 μM	[40]
poly(Toluidine blue O)/carbon nanotubes	Amperometry	0.001 ~ 4 mM	0.37 μM	[41]
polyoxometalate[PMO ₁₁ O ₃₉] ₇ /carbon nanocomposites	Amperometry	0.3 μM ~ 16 mM	0.3 μM	[42]
AuPd/UiO-66-NH ₂ metal-organic framework modified electrode	Amperometry	0.05 ~ 5666 μM/ 5666 ~ 15666 μM	0.01 μM	[43]
Au-Pt bimetallic nanoparticles/nitrogen-doped graphene	Amperometry	0.5 ~ 1621 μM	0.19 μM	[44]
Au-Pd nanostructures/reduced graphene oxide electrode	Amperometry	0.05 ~ 1000 μM	0.02 μM	[45]
horseradish peroxidase/porous Co ₃ O ₄ nanosheets/reduced graphene oxide	Amperometry	1 ~ 5400 μM	0.21 μM	[46]
PRhB/GCE	Amperometry	0.5 μM ~ 7.0 mM	0.1 μM	[17]
AuNPs/PRhB/MWCNTs/GCE	DPV/ Amperometry	1 ~ 25 μM 35 μM ~ 10 mM/ 0.1 ~ 5 μM 0.02~ 0.16 μM	6.7 nM	This work

Table 2. Determination of nitrite content in tap and lake water ($n = 5$)

Sample	Detected [μM]	Added [μM]	Found [μM]	Recovery [%]	RSD [%]
Tap water	0	2	2.09	104.5	3.51
		4	3.98	99.5	3.26
		6	6.05	100.8	2.67
Lake Water	1.42	2	3.40	99	3.45
		4	5.48	101.5	2.89
		6	7.45	100.5	2.53

4. CONCLUSION

In summary, this work demonstrated a simple electroanalytical method by modifying glassy carbon electrode with spherical Au nanoparticles, polyrhodamine B and nano-structural carbon nanotubes for the ultrasensitive determination of nitrite. The proposed AuNPs/PRhB/MWCNTs/GCE sensor exhibited superior electrocatalytic activity for the oxidation of nitrite with a high anodic current and a low oxidation over-potential. Meanwhile, multi-linear ranges for nitrite detection were obtained by DPV and amperometry with a wide linear range and an outstanding detection limit. Further, the prepared electrode has showed long-term stability, excellent selectivity, good reproducibility and can also be successfully applied for the detection of nitrite in real samples, which will provide a new platform for electrochemical detection of nitrite in environmental applications.

ACKNOWLEDGEMENTS

This work was supported by the Fundamental Research Funds for the Central Universities (No.17D111310) and the National Key Research and Development Program of China (Grant No. 2016YFC0400501).

References

1. W. Lijinsky and S. S. Epstein, *Nature*, 225 (1970) 21.
2. W. Frenzel, J. Schulz-Brüssel and B. Zinvirt, *Talanta*, 64 (2004) 278.
3. Z. Lin, X. Dou, H. Li, Y. Ma and J. M. Lin, *Talanta*, 132 (2015) 457.
4. H. Kodamatani, S. Yamazaki, K. Saito, T. Tomiyasu and Y. Komatsu, *J. Chromatogr. A*, 1216 (2009) 3163.
5. F. D. Betta, L. Vitali, R. Fett and A.C.O. Costa, *Talanta*, 122 (2014) 23.
6. H. Wang, F. F. Wen, Y. J. Chen, T. Sun, Y. Meng and Y. Zhang, *Biosens. Bioelectron.*, 85 (2016) 692.
7. B. Strehlitz, B. Gründig, W. Schumacher, P. M. H. Kroneck, K. D. Vorlop and H. Kotte, *Anal. Chem.*, 68 (1996) 807.
8. A. Afkhami, F. Soltani-Felehgari, T. Madrakian and H. Ghaedi, *Biosens. Bioelectron.*, 51 (2014) 379.

9. K. Dağcı and M. Alanyalloğlu, *Applied Mater. & interfaces*, 8 (2016) 2713.
10. J. Agrisuelas, D. Giménez-Romero, J. J. García-Jareño and F. Vicente, *Electrochem. Commun.*, 8 (2006) 549.
11. I. H. Kaplan, K. Dağcı and M. Alanyahoğlu, *Electroanalysis*, 22 (2010) 2694.
12. M. M. Barsan, E. M. Pinto and C. M.A. Brett, *Electrochim. Acta*, 53 (2008) 3973.
13. A. M. Chiorcea-Paquim, R. Pauliukaite and C. M. A. Brett, *Biosens. Bioelectron.*, 24 (2008) 297.
14. J. Dai, D. L. Deng, Y. L. Yuan, J. Z. Zhang, F. Deng and S. He, *Microchim. Acta*, 183 (2016)1553.
15. Y. J. Ma, M. Zhou, X.Y. Jin, B. Z. Zhang, H. Chen and N. Y. Guo, *Anal. Chim. Acta*, 464 (2002) 289.
16. H. Chen, M. Zhou, X. Y. Jin, Y. M. Song, Z. Y. Zhang and Y. J. Ma, *Anal. Chim. Acta*, 478 (2003) 31.
17. W. M. Wang, J. Leng, Y. F. Yu, L. M. Lu, L. Bai and X. L. Qiu, *Int. J. Electrochem. Sci.*, 9 (2014) 921.
18. D. J. Rao, Q. L. Sheng and J. B. Zheng, *Anal. Methods*, 8 (2016) 4926.
19. G. Zhao, K. Z. Liu, S. Lin, J. Liang, X.Y. Guo and Z. J. Zhang, *Microchim Acta*, 144 (2004) 75.
20. Y. Cui, C. Yang, W. Zeng, M. Oyama, W. Pu and J. Zhang, *Anal. Sci.*, 23 (2007) 1421.
21. X. Huang, Y. Li, Y. Chen and L. Wang, *Sens. Actuators. B*, 134 (2008) 780.
22. S. Zhang, Q. L. Sheng and J. B. Zheng, *New J. Chem.*, 40 (2016) 9672.
23. S. Iijima and T. Ichihashi, *Nature*, 363 (1993) 603.
24. A. Periasamy, W. Wu, G. Lin, Z. Shih, Z. Yang and H. Chang, *J. Mater. Chem.*, 2 (2014) 11899.
25. A. J. Bard, L. R. Faulkner, *Electrochemical Methods-Fundamentals and Applications*, John Wiley and Sons, New York, 2000.
26. C. E. Zou, B. B. Yang, D. Bin, J. Wang, S. M. Li, P. Yang, C. Q. Wang, Y. Shiraishi and Y. K. Du, *J. Colloid Interface Sci.*, 488 (2017) 135.
27. B. Thirumalraj, S.Palanisamy, S. M. Chen, D. H. Zhao, *J. Colloid Interface Sci.*, 478 (2016) 413.
28. G. Zhao, K. Z. Liu, S. Lin, J. Liang, X.Y. Guo and Z. J. Zhang, *Microchim Acta*, 144 (2004) 75.
29. Y. Cui, C. Yang, W. Zeng, M. Oyama, W. Pu and J. Zhang, *Anal. Sci.*, 23 (2007) 1421.
30. D. J. Rao, Q. L. Sheng and J. B. Zheng, *Anal. Methods*, 8 (2016) 4926.
31. S. Zhang, X. Y. Liu, N. Huang, Q. J. Lu, M. L. Liu, H. T. Li, Y. Y. Zhang and S. Z. Yao, *Electrochem. Acta*, 211 (2016) 36.
32. D. Liu, Q. H. Guo, X. P. Zhang, H. Q. Hou and T. Y. You, *J. Colloid Interface Sci.*, 450 (2015) 168.
33. F. Kuralay, M. Dumangöz and S. Tunç, *Talanta*, 144 (2015) 1133.
34. H. Bagheri, A. Hajian, M. Rezaei and A. Shirzamehr, *J. Hazard. Mater.*, 324 (2017) 762.
35. S. Radhakrishnan, K. Krishnamoorthy and C. Sekar, *Applied Catalysis B: Environ.*, 148-149 (2014) 22.
36. A. T. E. Vilian, V. Veeramani, S. M. Chen, R. Madhu, C. H. Kwak, Y. S. Huh and Y. K. Han, *Sci. Rep.*, 5 (2015) 1.
37. Z. Y. Bai, C. L. Zhou, N. Gao, H. J. Pang and H. Y. Ma, *RSC Adv.* 6 (2016) 937.
38. N. I. Lkhsan, P. Rameshkumar, A. Pandikumar, M. M. Shahid, N. M. Huang, S. V. Kumar and H. N. Lim, *Talanta*, 144 (2015) 908.
39. S. Zhang, B.Q. Li and J. B. Zheng, *Anal. Methods*, 7 (2015) 8366.
40. P. K. Rastogi, V. Ganesan and S. Krishnamoorthi, *J. Mater. Chem. A*, 2 (2014) 933.
41. D. Gligor and A. Walcarius, *J. Solid State Electrochem.*, 18 (2014) 1519-1528.
42. F. Boussema, R. Haddad, Y. Ghandour, M. S. Belkhiria, M. Holzinger, A. Maaref and S. Cosnier, *Electrochem. Acta*, 222 (2016) 402.
43. J. Yang, L. T. Yang, H. L. Ye, F. Q. Zhao and B. Z. Zeng, *Electrochem. Acta*, 219 (2016) 647.
44. Z. Li, Z. Z. An, Y. Y. Guo, K. N. Zhang, X. L. Chen, D. X. Zhang, Z. H. Xue, X. B. Zhou and X. Q. Lu, *Talanta*, 161 (2016) 713.

45. S. S. Li, Y. Y. Hu, A. J. Wang, X. X. Weng, J. R. Chen and J. J. Feng, *Sens. Actuators B*, 208 (2015) 468.
46. H. Liu, K. Guo, J. Lv, Y. Gao, C. Y. Duan and Z. F. Zhu, *Sens. Actuators B*, 238 (2017) 249.

© 2017 The Authors. Published by ESG (www.electrochemsci.org). This article is an open access article distributed under the terms and conditions of the Creative Commons Attribution license (<http://creativecommons.org/licenses/by/4.0/>).